# Stoichiometry-Driven Formation of Two-Dimensional Ternary Oxides: From Quasicrystal Approximants to Honeycomb Lattice Structures

Catalina Ruano-Merchan, Vipin Kumar Singh, Olivier Copie, Stéphane Andrieu, Ludovic Pasquier, Muriel Sicot, Julian Ledieu, Vincent Fournée

**TOC Graphic**

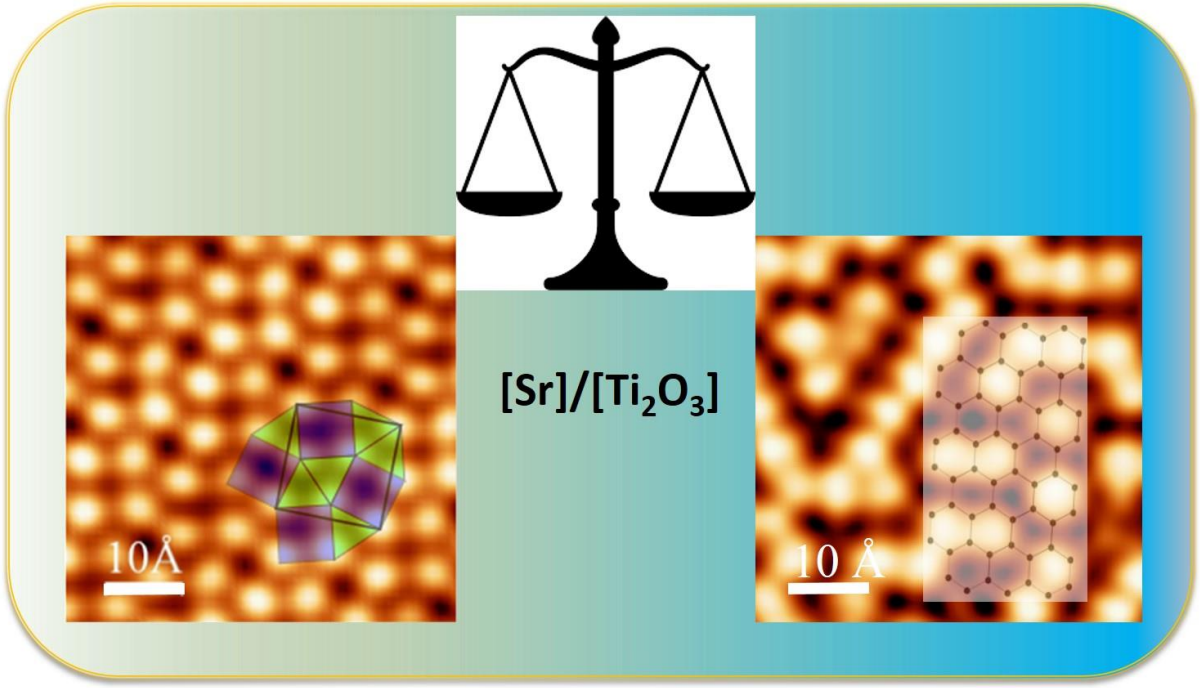

# Stoichiometry-driven formation of 2D ternary oxides: from quasicrystal approximant to honeycomb lattices structures.

C. Ruano-Merchan, V. K. Singh, O. Copie, S. Andrieu, L. Pasquier, M. Sicot, J. Ledieu, and V. Fournée*

*Institut Jean Lamour, UMR7198 CNRS-Nancy-Université de Lorraine, Campus ARTEM - 2 allée André Guinier, BP 50840, 54011 Nancy, France*

Corresponding author. *E-mail address*: vincent.fournee@univ-lorraine.fr

## Abstract

The spontaneous ordering of a two dimensional (2D) $SrTiO_3$-derived film supported on $Pt(111)/Al_2O_3(0001)$ is investigated by scanning tunneling microscopy. After annealing under ultra-high vacuum, a 2D reduced wetting layer is formed where oxide quasicrystal approximants are observed. Upon increasing the number of preparation cycles, the Sr content in the film decreases. The structure of the film then evolves into a $Ti_2O_3$ honeycomb (HC) lattice partially decorated by Sr adatoms. The latter are localized in hollow sites of the network with several complex structures resulting from the Sr occupation rate. A labyrinth-like phase was identified as well as an ordered $(\sqrt{3}x\sqrt{3})R30°$ phase where only 1/3 of the hollow sites of the HC lattice are occupied. Those results suggest that the phase sequence is driven by a stoichiometry change that is mainly controlled by the $Sr/(Ti_2O_3)$ ratio.

## Keywords

2D oxides; quasicrystals; approximants; honeycomb lattices.

## Introduction

When approaching the two-dimensional (2D) limit, oxides are known to exhibit structures and properties that strongly depart from those of their respective bulk counterparts [1, 2]. They are promising materials for both fundamental science and technological applications [3, 4]. Novel 2D phases derived from ternary oxide thin films grown on metal substrates have been reported in the last decade, exhibiting complex crystallographic structures [1, 2, 5]. The most extreme examples are the two-dimensional oxide quasicrystals (OQCs) exhibiting twelve-fold rotational symmetry that have been discovered by reduction of $BaTiO_3$ perovskite oxide thin films epitaxially grown on a Pt(111) single crystal substrate [6, 7]. An isostructural OQC was reported later in the Sr-Ti-O/Pt(111) system [8]. These long-range ordered structures with dodecagonal symmetry are described by a specific triangle-square-rhomb tiling known as the Niizeki-Gähler tiling (NGT) [9]. The bright protrusions observed by scanning tunneling microscopy (STM) in Ba-Ti-O or Sr-Ti-O supported on Pt(111) substrate reproduce such an aperiodic tiling. Beside the OQCs, other related phases known as quasicrystalline approximants have also been reported [8, 10, 11, 12]. They are periodic structures consisting of the same tiling elements but occurring in different ratio and arranged in slightly different ways. Approximants of different structural complexities have been reported, ranging from a small square unit cell called the σ phase with 4:2:0 triangles:squares:rhombi respectively per unit cell in the Ba-Ti-O system [10], up to the giant square approximant reported recently with 48:18:6 tiles in the unit cell in the Sr-Ti-O system [13, 14]. All these phases are obtained by reduction of perovskite oxide thin films supported on metal through a high temperature annealing cycle under ultra-high vacuum (UHV) conditions. Under annealing in $O_2$, the thin films first undergo a dewetting step leading to the formation of 3D oxide islands on the bare metal substrate [7]. Upon further annealing in UHV at higher temperature, a continuous layer of a reduced oxide spreads to fully cover the metal support. Despite many previous investigations, the exact structure of these novel complex 2D oxides was still controversial until recently [13-18]. Using the tile decoration proposed by Cockayne *et al.* for the Ba-Ti-O/Pt(111) system and applying it to the tiling scheme determined experimentally for the 48:18:6 giant square approximant discovered in the Sr-Ti-O/Pt(111) system, a structural model could be proposed in Ruano *et al*. [13]. Simulated STM images based on density functional theory (DFT) calculations using this model were found in excellent agreement with the experimental ones. The bright protrusions decorating the tiling vertices observed in STM images are attributed to the slightly protruding Sr atoms and not to the Ti sublattice as previously thought. This chemical tiling decoration was recently confirmed for the 48:18:6 giant square approximant based on surface x-ray diffraction experiments combined with additional DFT calculations [14]. The same tiling decoration was also successfully applied to build a model for another large hexagonal approximant in the same system, allowing for a structural solution of the directly related OQC and all related approximant phases [13]. In the model, each Ti atom is bound to three O atoms and each O atom is located between two Ti atoms. The mean vertical distance between the topmost Pt atoms and the Ti atoms is much smaller (2.3 Å) than that of O or Sr atoms (3.1 Å and 3.2 Å, respectively). The rumpling of the supported oxide layer is associated with charge transfer mechanisms from the most electropositive elements (Sr, Ti) towards the most electronegative ones (Pt and O). The global chemical compositions of the giant square and hexagonal approximant are $Sr_{0.36}TiO_{1.54}$ and $Sr_{0.38}TiO_{1.56}$ respectively, both being very close to that of the ideal OQC $Sr_{0.37}TiO_{1.55}$ using the same tiling decoration scheme.

In a recent publication by Schenk *et al.* [14], it was proposed that the structure of the 48:18:6 approximant can be understood as a partially Sr-decorated $Ti_2O_3$ honeycomb (HC) lattice containing specific defects, that modify $Ti_6O_6$ rings into $Ti_nO_n$ rings with n=4, 7 and 10. DFT calculations suggest that such transformations of the $Ti_2O_3$ honeycomb are driven by electrostatic interactions between positively charged Sr atoms. On the other hand, Wu *et al*. have investigated $Ba_xTi_2O_3$ ultrathin films by evaporating small amounts of Ba on a previously formed $Ti_2O_3$ HC on Au(111) substrates ($0 \leq x \leq 2/3$) [19]. Indeed, various 2D transition metal oxides are known to adopt honeycomb geometry when supported on metal substrates [19-21]. It was shown by STM and theoretical calculations that Ba atoms adsorb individually on hollow sites of the $Ti_2O_3$ HC network [19]. Depending on the Ba coverage, different ordered and disordered phases have been identified. Here again, the range of the dipolar interactions between Ba adatoms is the key factor to understand the phase formation and properties. The composition of these phases ranges from $Sr_0TiO_{1.5}$ to $Sr_{0.33}TiO_{1.5}$, *i.e.* on the Sr poor side of the OQC approximants.

Here, we report the spontaneous transformation of 2D quasicrystalline approximants described by square-triangle-rhomb tilings into $Ti_2O_3$ HC lattices partially decorated with Sr atoms upon repeated reduction-oxidation cycles in UHV. The phase sequence is associated with a change in the layer stoichiometry, mainly the progressive depletion of Sr that drives the phase transformations.

## Experimental procedure

An $Al_2O_3$(0001) substrate (SurfaceNet GmbH) was first degassed at 1173 K in UHV for 15 minutes. A 10 nm thick buffer layer of Pt(111) was subsequently grown by molecular beam epitaxy (MBE) with the substrate held at a temperature of 673 K. The growth was monitored by reflection high-energy electron diffraction (RHEED). Then an ultra-thin film of $SrTiO_3$ (0.8 nm) was grown by pulsed laser deposition (PLD) on the Pt buffer layer using a KrF excimer laser (248 nm) at 1 Hz pulse repetition and a fluence of 0.4 $J.cm^{-2}$ (sample A). Two other films were also investigated consisting of (5 nm) $SrTiO_3$/(1 nm) Ti/(10 nm) Pt(111)/$Al_2O_3$(0001) (sample B) and (0.4 nm) $SrTiO_3$/(10 nm) Pt(111)/$Al_2O_3$(0001) (sample C), both grown under similar conditions as sample A. No obvious correlations could be evidenced between the different thicknesses of the deposited $SrTiO_3$ films and the resulting structure of the Sr-Ti-O rewetting layer. The role of the 1 nm thick Ti layer in sample B is to promote the formation of a solid solution with Pt upon annealing that possesses a slightly different lattice parameter compared to pure Pt, in order to favor the epitaxial growth of $SrTiO_3$(111) due to a smaller lattice mismatch. The film stacking was fully characterized *in situ* by RHEED and *ex situ* by high-resolution x-ray diffraction as described in detail in Ref. [13]. The $SrTiO_3$ films are stable under ambient conditions, which allowed for sample transfer through air. Thus, in a second UHV platform, oxidation-reduction cycles were performed after a first annealing at 900 K under $1\times10^{-6}$ mbar of $O_2$ to remove carbon surface contamination. The reduction step consists of further annealing of the film stacking up to ~ 1123 K under UHV conditions ($<10^{-8}$ mbar). The experimental setup is equipped with an e-beam heater and *in situ* surface characterization techniques including low energy electron diffraction (LEED) and variable temperature STM. The STM images were recorded at room temperature under various bias $V_b$ and tunneling current $I_t$ (occupied electronic states of the sample are probed at $V_b>0$). The background pressure of the

experimental chamber was about $5\times10^{-10}$ mbar. The temperature was monitored with a bichromatic pyrometer. STM images were processed with the WSxM software [22].

## Results

Following the first oxidation-reduction cycle of the thin film stacking (sample A), a reduced 2D oxide wetting layer was formed exhibiting OQC approximants. Two different phases were previously reported in Ref. [13] in sample A, including a giant square approximant with a lattice parameter equal to 44.4 Å and an hexagonal approximant with a lattice parameter equal to 28 Å. Their unit cell could be described by two different tilings constructed with the same square, triangle and rhombus tiles, with a common edge length of about 6.7 Å. The unit cell of the giant square approximant contains 72 tiles, while that of the hexagonal one contains 29 tiles. Another smaller size approximant known as the σ-approximant could be observed on sample B after two annealing cycles in vacuum ($1x10^{-8}$ mbar) at 1173 K for 15 min. The formation of the σ-phase approximant was reported before in the $BaTiO_3$/Pt(111) and $BaTiO_3$/Ru(0001) systems [10,11], but not in the $SrTiO_3$/Pt(111). STM images of this phase are shown in Fig. 1. It shows a periodic pattern with a square unit mesh as evidenced by the fast-Fourier transform (FFT) of the STM image, with lattice dimensions equal to 12.5 ± 0.2 Å. Each unit cell consists of two square and four triangle tiles. The common edge length of the tiles is 6.4 ± 0.1 Å, a value slightly smaller than the average distance of 6.7 Å between protrusions previously reported for the σ-phase approximant in $BaTiO_3$/Pt(111) [10]. This is consistent with the fact that the lattice constant of $SrTiO_3$ is smaller by 2% compared to that of $BaTiO_3$. In addition, some modulation of the STM contrast can be seen at large scale (Fig. 1(a)), producing a moiré structure with a periodicity equal to 2.9 ± 0.2 nm. This leads to additional spots in the experimental FFT (Fig.1(c)). The moiré structure was identified as a higher-order commensurate structure with respect to the Pt(111) substrate, with either a $\begin{pmatrix} 27 & 10 \\ 3 & 20 \end{pmatrix}$ or a $\begin{pmatrix} 19 & -16 \\ 19 & 16 \end{pmatrix}$ matrix superstructure [10, 11], which cannot be distinguished from STM alone.

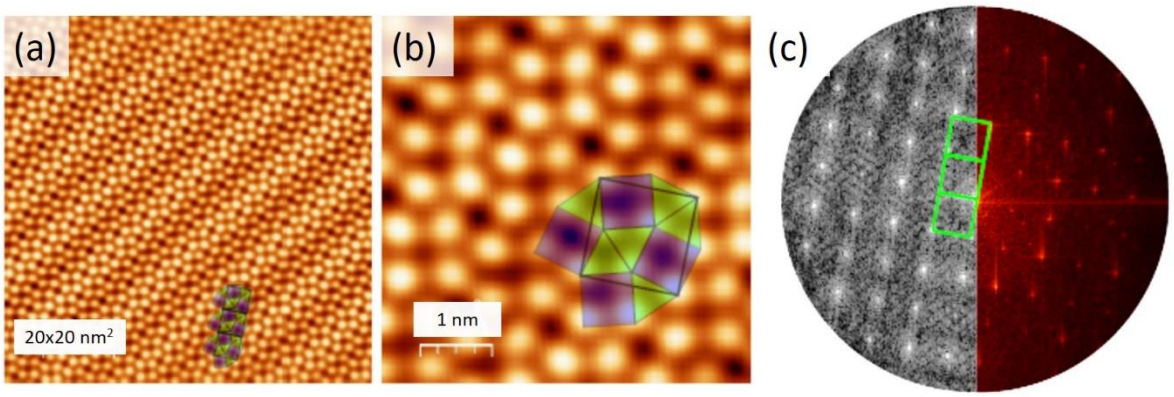


Figure 1: (a) Atomically resolved STM image (20x20 $nm^2$, $V_b$ =1.5 V, $I_t$ =0.2 nA) of the σ-phase observed on sample B, (b) Zoom of image (a) (5x5 $nm^2$) showing the tiling description of the unit cell, (c) Calculated (left) and experimental (right) FFT of the STM image in (a).

Upon further annealing cycles under similar conditions, the wetting layer undergoes several structural transitions as revealed by LEED (not shown here) and STM. Figure 2(a) shows an

STM image of a labyrinthic phase consisting in bright dots distributed on a HC lattice. The hollow sites of the HC lattices are not all occupied, resulting in a disordered appearance. The height profile along the blue line in Fig. 2(b) indicates a height difference of 1.1 Å between the top of the bright dots and the bottom of the HC lattice. The shortest distance between adjacent bright dots is 5.5 Å (Fig. 2(c)). The height distribution of the topographic image in Fig. 2(a) shows two peaks separated by a height difference of 0.7 Å corresponding to the height difference between the honeycomb lattice and the protruding atoms (Fig. 2(d)). The observed pattern is similar to the one reported by Wu *et al.* for a $Ti_2O_3$ HC lattice grown on Au(111) substrate and partially decorated with Ba atoms [19]. By analogy, we make the hypothesis that the bright protrusions are Sr atoms protruding on a $Ti_2O_3$ HC supported on the Pt(111) buffer layer surface.

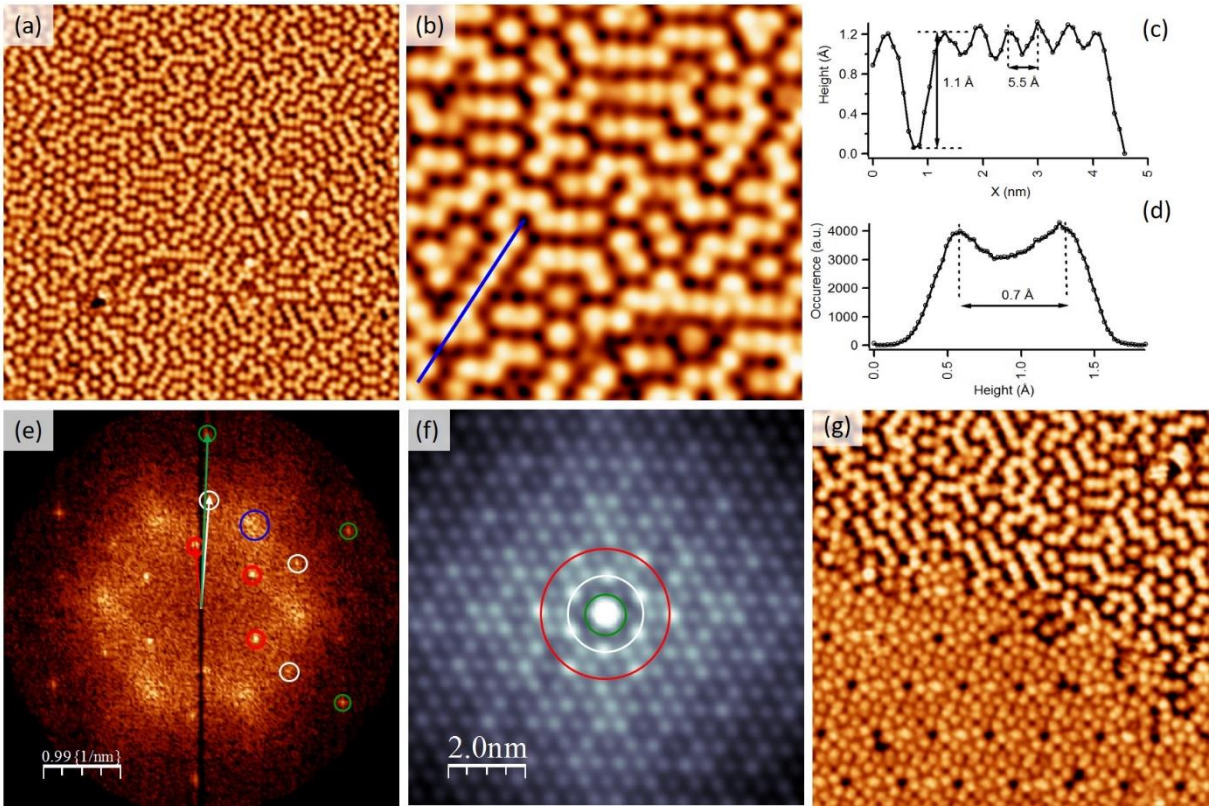


Figure 2: (a) Atomically resolved STM image (30x30 $nm^2$, $V_b$ =1.5 V, $I_t$ =0.2 nA) of the labyrinth-like phase, (b) Zoom of image (a) (10x10 $nm^2$), (c) Height profile along the line drawn in (b), (d) Height histogram of a surface topographic image as in (a). (e, f) Calculated FFT and autocorrelation of the STM image in (a). Three hexagonal lattices are identified and indicated by the red, white and green circles in (e). They correspond to the intensity maxima highlighted by colored circles in the autocorrelation image in (f). (g) Atomically resolved STM image of the large hexagonal OQC approximant coexisting with the labyrinth-like phase (20x20 $nm^2$, $V_b$ =1.5 V, $I_t$ =0.2 nA)

Figure 2(e) is the FFT of the STM image in Fig. 2(a). Three different hexagonal lattices are identified (red, white and green circles), corresponding to lattice parameters equal to 14.9 ± 0.3 Å, 9.1 ± 0.2 Å and 5.5 ± 0.1 Å, respectively. The white and green lattices are rotated by 7° ± 1° and 5° ± 1° with respect to the red one. This may be due to a small rotation of the lattice formed

by the protrusions with respect to that of the underlying HC lattice. The green reciprocal lattice vector in Fig. 2(e) is the sum of the red and white vectors. The lattice parameter equal to 5.5 Å corresponds to the shortest distance between adjacent bright dots in the STM images and it matches the lattice parameter of the underlying honeycomb lattice. A similar value has been reported for $Ti_2O_3$ HC on Au(111) [19]. Other distances correspond to higher order nearest neighbor distances on the HC lattice. The autocorrelation of the STM image in Fig. 2(f) is also consistent with a random occupation of the underlying HC lattice. Figure 2(g) shows an STM image recorded at a different area of the surface where the labyrinth-like phase coexists with the previously reported large hexagonal approximant [13]. This is corroborated by the LEED patterns (not shown) indicating that different structures coexist at the surface with different weight, depending on the sample position. These inhomogeneities could result from an inhomogeneous surface temperature during the annealing as part of the sample is directly heated by e-beam (Ta sample plate with a window), or due to local density variations and slow kinetics.

Upon further annealing cycles, STM images reveal a different 2D ordering and a lower density of bright protrusions as can be seen in Fig. 3(a). The bright protrusions (attributed to Sr atoms) are now occupying the hollow sites of the HC lattice in an ordered way, forming a (√3x√3)R30° phase on the HC lattice. The corresponding FFT is shown in Fig. 3(b), where the two hexagonal patterns can be identified. The first lattice (green vector) corresponds to a measured lattice parameter similar to that of the honeycomb previously determined (5.5 ± 0.1 Å), within the accuracy of the STM measurement. The second lattice (white vector) corresponds to the (√3x√3)R30° phase formed by the bright protrusions in the STM images, with a lattice parameter of 9.9 ± 0.2 Å. Assuming that the bright protrusions are Sr atoms decorating the $Ti_2O_3$ HC, the (√3x√3)R30° phase has a smaller Sr content compared to the labyrinth-like phase. Note that the (√3x√3)R30° phase contains defects, like vacancies, adatoms, line shifts and domain boundaries, implying Sr mobility upon annealing.

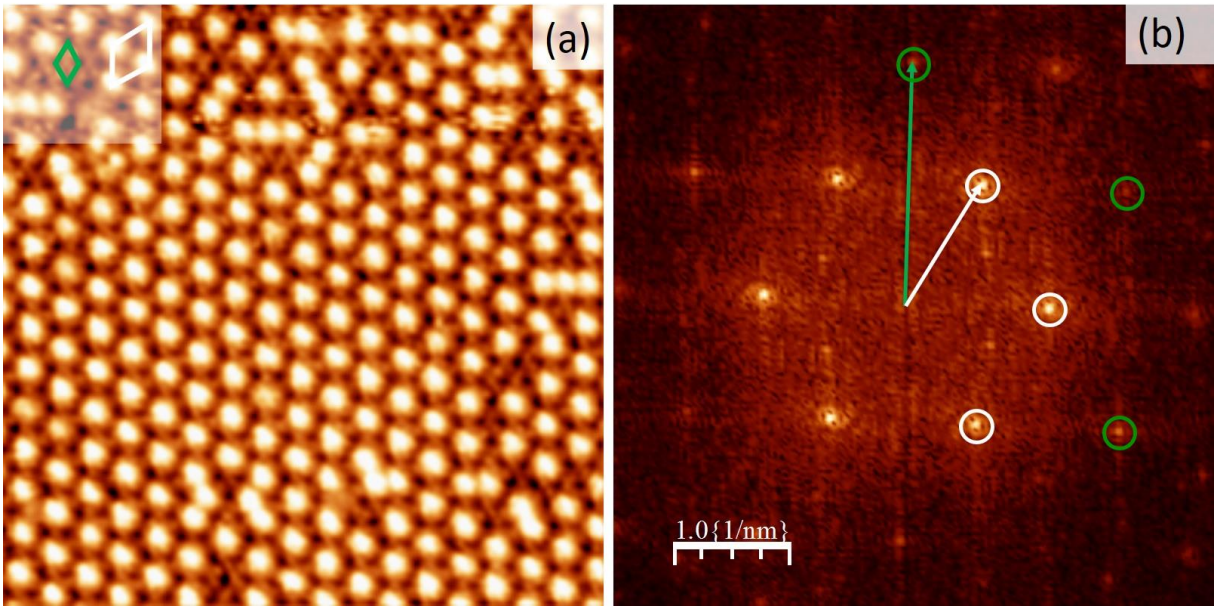


Figure 3: (a) Atomically resolved STM image (15x15 $nm^2$, $V_b$ = -1.5 V, $I_t$ =0.2 nA) of the (√3x√3)R30° phase on the HC lattice. The corresponding two surface unit cells are shown in white and green respectively. (b) FFT of the STM image in (a).

**Discussion**

The Sr coverage (x) can be estimated from the STM images by counting the number of Sr atoms (bright protrusions) occupying the hollow sites of the $Ti_2O_3$ HC lattice. For full Sr occupation x = 1, the ratio Sr:Ti:O will be 0.5:1:1.5. The Sr coverage and the corresponding calculated stoichiometry are x = 0.47; 0.23:1:1.5 and x = 0.33; 0.16:1:1.5 for the labyrinth-like phase and the (√3x√3)R30° phase respectively. The (√3x√3)R30° phase corresponds to the situation in which all second nearest neighbor sites of a given hollow site are occupied by a Sr atom and all first neighbor sites are empty (*i.e.* 1/3 occupancy of the HC hollow sites). These values are consistent with the previous report by Wu *et al.* for Ba adsorbed on $Ti_2O_3$ HC lattice on Au(111) (x=0.49 and x=0.35 for the similar labyrinth-like and (√3x√3)R30° phases respectively) [19]. Moreover, Wu *et al.* stated that "STM images for coverages exceeding x = 2/3 indicate that a completely different type of atomic ordering takes place where Ba no longer adsorbs on the $Ti_2O_3$ HC hollow sites" [19]. Indeed, the equivalent Sr coverage and the corresponding stoichiometry of the previously reported OQC approximants are x = 0.72; 0.36:1:1.54 for the giant square approximant; x = 0.76; 0.38:1:1.56 for the large hexagonal approximant; and x = 0.66; 0.33:1:1.55 for the σ-phase approximant. These chemical compositions are deduced from the tiling description of each surface unit cell and the chemical decoration of the generic triangles, square and rhombus tiles ($SrTiO_3$, $SrTi_4O_4$ and $SrTi_2O_2$ respectively) as determined previously [15]. The compositions of the two large approximants are very close to that of the ideal Niizeki-Gähler tiling describing the quasicrystalline phase (0.37:1:1.55).

From these estimated chemical compositions, it can be concluded that the structural transformations observed in the 2D oxide layer are driven by stoichiometry changes occurring after repeated annealing cycles. The phase sequence and compositions are summarized in Fig. 4. In that sequence, we also include the previously reported dodecagonal phase [8], which was observed in sample C after sequential annealing in $O_2$ at 903 K for 15 minutes and UHV annealing at 1158 K for 5 minutes. While the Ti/O ratio remains almost the same for all phases, the Sr content progressively decreases along the phase sequence. Note that several approximant phases can co-exist at the surface due to samples inhomogeneities and therefore the phase sequence experimentally observed may not strictly obey the sequence illustrated in Fig. 4. The exact reason for Sr depletion would be difficult to identify unambiguously, as Sr atoms may diffuse in the bulk, or evaporate in the gas phase during UHV annealing at high temperature, or being trapped in stable oxide islands of higher Sr stoichiometry during the intermediate oxidation cycles.

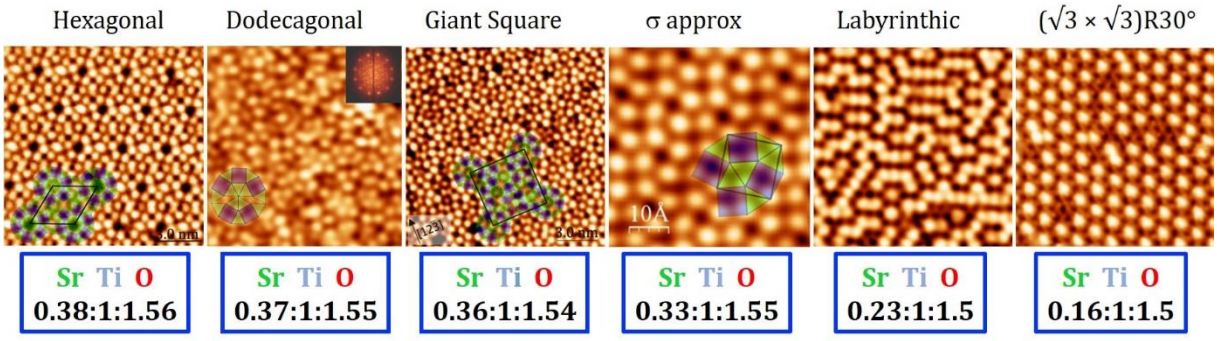


Figure 4: STM snapshots of the different 2D oxide phases observed upon repeated annealing cycles of the $SrTiO_3$/Pt(111)/$Al_2O_3$(0001) stacking and their derived chemical compositions.

It was recently proposed that the structure of the OQC and approximants can be understood as a partially Sr-decorated $Ti_2O_3$ honeycomb lattice containing specific defects, that modify $Ti_6O_6$ rings into $Ti_nO_n$ rings with n=4, 7 and 10, occupied by 0, 1 or 2 Sr atoms respectively [14]. The mechanism that converts HC lattices into square-triangle-rhombus tilings is based on Stone-Wales transformations. DFT calculations suggest that such transformations of the $Ti_2O_3$ honeycomb are driven by electrostatic interactions between positively charged Sr atoms occupying the hollow sites of the HC lattice, as the transformations of $Ti_6O_6$ rings into $Ti_nO_n$ rings lead to an increased separation of the positively charged Sr atoms. Our experimental results suggest that upon repeated annealing in UHV, the density of Sr surface atoms decreases resulting in a reduction of the electrostatic repulsion at the origin of the Stone-Wales transformations. As a result, the square-triangle-rhombus tilings spontaneously transform into Sr decorated HC lattices, passing through a sequence of phases as illustrated in Fig. 4. Inversely, dosing Sr atoms on a pristine $Ti_2O_3$ honeycomb lattice should lead to the inverse phase sequence and is considered as a new fabrication method to explore complex 2D oxide phases [23].

## Conclusions

In summary, we reported the continuous transformation of 2D oxide quasicrystalline approximants derived from $SrTiO_3$(111) ultrathin film supported on Pt(111)/$Al_2O_3$(0001) into partially Sr-decorated $Ti_2O_3$ honeycomb lattices upon high temperature UHV annealing. Three different approximant phases have been identified as the giant square, the large hexagonal and the modulated σ phases, as well as the dodecagonal phase. All these phases have a structure based on square-triangle-rhombus tilings. Upon further annealing, other ordered structures based on partially Sr-decorated HC lattice were observed (labyrinthic and ($\sqrt{3}$x$\sqrt{3}$)R30° phases). The structural transformations are driven by stoichiometry changes occurring after repeated annealing cycles. While the Ti/O ratio remains almost the same for all phases, the Sr content progressively decreases, probably due to Sr atoms either diffusing in the bulk, or evaporating in the gas phase during UHV annealing at high temperature, or being trapped in stable oxide islands of higher Sr stoichiometry during the intermediate oxidation cycles.". It has been suggested that Sr-decorated $Ti_2O_3$ honeycomb lattices can transform into square-triangle-rhombus tilings upon increasing Sr content through the creation of Stone-Wales defects, driven by electrostatic forces. The results presented here are consistent with this idea and show that this process is reversible. The decrease in Sr surface atom density results in a reduction of the electrostatic repulsion between positively charged alkaline earth metal atoms. As a result, the square-triangle-rhombus tilings spontaneously transform into decorated HC lattices. Fine tuning of the [Sr]/[$Ti_2O_3$] ratio should allow to explore the complex phase diagram in these 2D oxides in a systematic way. This may also be an interesting approach for tailoring well-terminated surface for the regulated growth of (111)-oriented perovskite oxides.

## Acknowledgments

This work was supported by the European Integrated Center for the Development of New Metallic Alloys and Compounds (ECMetAC) and the ANR NOUS (ANR-21-CE09-0005-01). Access to equipment's from the "DAUM" platform of the Jean Lamour Institute is acknowledged.

## Data availability statement

Data sets generated during the current study are available from the corresponding author on reasonable request.

## References


[1] Barcaro, G.; and Fortunelli, A. 2D oxides on metal materials: concepts, status, and perspectives. *Phys. Chem. Chem. Phys.*, **2019**, *21*, 11510-11536.

[2] Netzer, F.P.; and Fortunelli A. Oxide materials at the two-dimensional limit, Springer, Switzerland (2016).

[3] Heard, C.J.; Cějka, J.; Opanasenko, M.; Nachtigall, P.; Centi, G.; Perathoner, S. 2D Oxide Nanomaterials to Address the Energy Transition and Catalysis, *Adv. Mater.*, **2019**, *31*, 1801712.

[4] Santander-Syro, A. F.; Copie, O.; Kondo, T.; Fortuna, F.; Pailhès, S.; Weht, R.; Qiu, X. G.; Bertran, F.; Nicolaou, A.; Taleb-Ibrahimi, A.; *et al.* Two-dimensional electron gas with universal subbands at the surface of $SrTiO_3$, *Nature*, **2011**, *469*, 189–193.

[5] Förster, S.; and Widdra, W. in *Oxide Materials at the Two- Dimensional Limit*, eds. Netzer F. P. and Fortunelli A., Springer, Switzerland, 2016.

[6] Förster, S.; Meinel, K.; Hammer, R.; Trautmann, M.; and Widdra W. Quasicrystalline structure formation in a classical crystalline thin-film system, *Nature*, **2013**, *502*, 215–218.

[7] Förster, S.; Flege, J. I.; Zollner, E. M.; Schumann, F. O.; Hammer, R.; Bayat, A.; Schindler, K. M.; Falta, J.; and Widdra W. Growth and decay of a two-dimensional oxide quasicrystal: High-temperature in situ microscopy, *Ann. Phys.*, **2017**, *529*, 1600250.

[8] Schenk, S.; Förster, S.; Meinel, K.; Hammer, R.; Leibundgut, B.; Paleschke, M.; Pantzer, J.; Dresler, C.; Schumann, F. O.; and Widdra, W. Observation of a dodecagonal oxide quasicrystal and its complex approximant in the $SrTiO_3$/Pt(111) system, *J. Phys.: Condens. Matter*, **2017**, *29*, 134002.

[9] Gähler, F. *Crystallography of dodecagonal quasicrystals, in Quasicrystalline materials: Proceedings of the I. L. L. Workshop*, ed. Janot C., World Scientific, Singapore, 1988, pp. 272–284.

[10] Förster, S.; Trautmann, M.; Roy, S.; Adeagbo, W.; Zollner, E.; Hammer, R.; Schumann, F.; Meinel, K.; Nayak, S.; Mohseni, K.; Hergert, W.; Meyerheim, H.; and Widdra, W.; Observation and structure determination of an Oxide quasicrystal approximant, *Phys. Rev. Lett.*, **2016**, *117*, 095501.

[11] Zollner, E.M.; Schuster, F.; Meinel, K.; Stötzner, P.; Schenk, S.; Allner, B.; Förster, S.; Widdra, W, Two-Dimensional Wetting Layer Structures of Reduced Ternary Oxides on Ru(0001) and Pt(111), *Phys. Status Solidi B*, **2020**, *257*, 1900655.

[12] Maniraj, M.; Tran, L. V.; Krahn, O.; Schenk, S.; Widdra, W.; and Förster, S. Hexagonal approximant of the dodecagonal oxide quasicrystal on Pt(111), *Phys. Rev. Materials*, **2021**, *5*, 084006.

[13] Ruano Merchan, C. ; Dorini, T. T.; Brix, F. ; Pasquier, L.; Jullien, M.; Pierre, D.; Andrieu, S.; Dumesnil, K.; Parapari, S. S.; Šturm S.; *et al.* Two-dimensional square and hexagonal oxide quasicrystal approximants in $SrTiO_3$ films grown on $Pt(111)/Al_2O_3(0001)$, *Phys. Chem. Chem. Phys.*, **2022**, **24** 7253.

[14] Schenk, S.; Krahn, O.; Cockayne, E.; Meyerheim, H.L.; de Boissieu, M.; Förster S.; and Widdra W. 2D honeycomb transformation into dodecagonal quasicrystals driven by electrostatic forces, *Nature Comm.* **2022**, *13*, 7542.

[15] Cockayne, E.; Mihalkovic M.; and Henley C. L. Structure of periodic crystals and quasicrystals in ultrathin films of Ba–Ti–O, *Phys. Rev. B*, **2016**, *93*, 020101.

[16] Förster, S.; Schenk, S.; Zollner, E.M.; Krahn, O.; Chiang, C-T.; Schumann, F.O.; Bayat, A.; Schindler, K-M.; Trautmann, M.; Hammer, R.; *et al.* Quasicrystals and their approximants in 2D ternary oxides, *Phys. Status Solidi B*, **2020**, *257*, 1900624.

[17] Li , X.; Horiba, K.; Sugiura, R.; Yamada, T.; Yuhara, J. Growth of Ba–O ultrathin films on Pt(111) followed by Ti incorporation to prepare oxide crystalline approximants and quasicrystals, *Applied Surface Science*, **2021**, *561*, 150099.

[18] Yuhara, J.; Horiba, K.; Sugiura, R.; Li , X.; Yamada, T. Growth and composition of an ultrathin Ba-Ti-O quasicrystal film and its crystalline approximant on Pt(111). *Phys. Rev. Mat.*, **2020**, *4*, 103402.

[19] Wu, C. Castell, M.R. Goniakowski, J. and Noguera, C. Stoichiometry engineering of ternary oxide ultrathin films: $Ba_xTi_2O_3$ on Au(111). *Phys. Rev. B*, **2015**, *91*, 155424.

[20] Wemhoff, P. I.; Nilius, N.; Noguera, C.; and Goniakowski J. Two-Dimensional Oxide Alloys Probed at the Atomic Level: $(V,Fe)_2O_3$ Honeycomb Monolayers on Pt(111). *J. Phys. Chem. C*, **2022**, *126*, 5070−5078.

[21] Wemhoff, P. I.; Noguera, C.; Goniakowski, J.; and Nilius, N. Structure and Stoichiometry Self-Organization in a Mixed Vanadium−Iron Oxide Honeycomb Film on Ru(0001). *J. Phys. Chem. C*, **2022**, *126*, 19947−19955.

[22] Horcas, I.; Fernandez, R.; Gomez-Rodriguez, J. M.; Colchero, J.; Gomez-Herrero J.; and Baro, A. M. WSXM: A software for scanning probe microscopy and a tool for nanotechnology, *Rev. Sci. Instrum.*, **2007**, *78*, 013705.

[23] Haller, M.; Schenk, S.; Förster S.; and Widdra, W. in *Proceedings of International Conference on Complex Orders in Condensed Matter: aperiodic order, local order, electronic order, hidden order*. Evian, Sept. 2023.